

Personalized Generative Low-light Image Denoising and Enhancement

Xijun Wang, Prateek Chennuri, Yu Yuan, Bole Ma, Xingguang Zhang, Stanley Chan
Purdue University

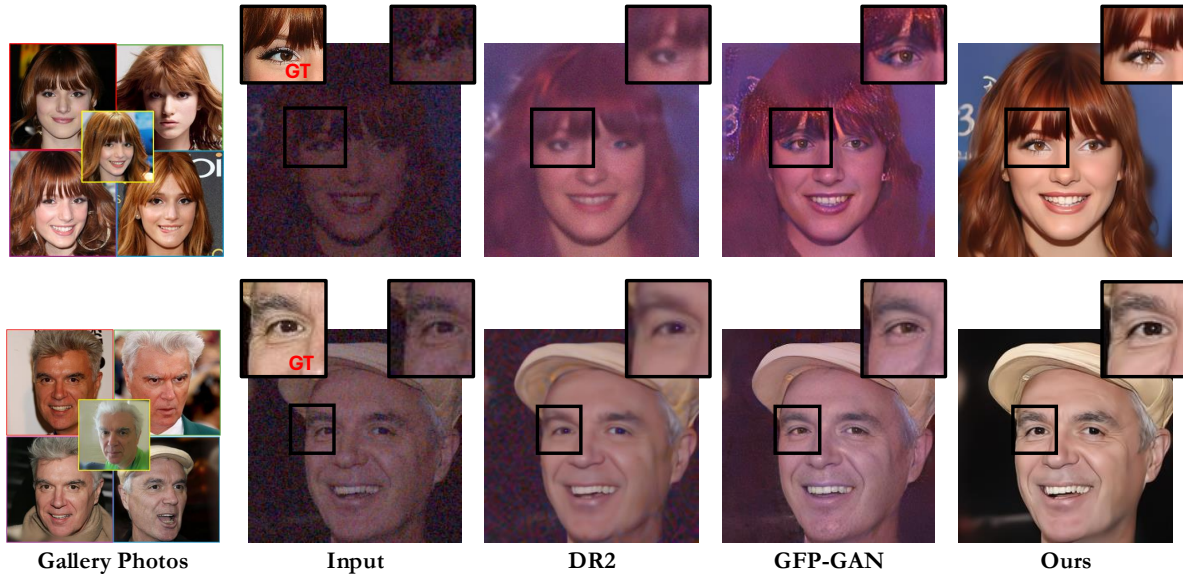


Figure 1. Using gallery photos from a user’s smartphone, we can restore low-light, noisy facial images. Our method produces finer details and better identity compared to current state-of-the-art face restoration approaches like DR2 [53] and GFP-GAN [50].

Abstract

While smartphone cameras today can produce astonishingly good photos, their performance in low light is still not completely satisfactory because of the fundamental limits in photon shot noise and sensor read noise. Generative image restoration methods have demonstrated promising results compared to traditional methods, but they suffer from hallucinatory content generation when the signal-to-noise ratio (SNR) is low. Recognizing the availability of personalized photo galleries on users’ smartphones, we propose *Personalized Generative Denoising (PGD)* by building a diffusion model customized for different users. Our core innovation is an identity-consistent physical buffer that extracts the physical attributes of the person from the gallery. This ID-consistent physical buffer provides a strong prior that can be integrated with the diffusion model to restore the degraded images, without the need of fine-tuning. Over a wide range of low-light testing scenarios, we show that

PGD achieves superior image denoising and enhancement performance compared to existing diffusion-based denoising approaches.

1. Introduction

With the astonishing development of smartphones, it is safe to say that smartphone cameras today have surpassed digital single-lens reflex (DSLR) cameras in both popularity and functionality. However, the small form factor of smartphone cameras puts a tight constraint on the aperture size, hence limiting the amount of light a CMOS pixel can detect. In a low-light imaging environment, this creates a fundamental limitation to how short the minimum exposure needs to be and how much signal-to-noise ratio (SNR) the sensor can support. While some of the noise seen at low light can be mitigated using better CMOS technology (e.g., correlated double sampling to reduce the read noise [40] and deep-well pump gate to reduce the stray capacitance between the floating diffusion and the transfer gate [38, 39]), the Poisson / Bose-Einstein statistics due to random photon arrivals is

[†]Project page: <https://genai-restore.github.io/DiffPGD/>.

a problem created by mother nature that cannot be solved by even the ideal sensors. Therefore, image denoising and enhancement by exploiting the internal structures of images become a necessary task for all smartphone cameras.

From a signal-processing perspective, degradation caused by low light can be roughly approximated via

$$y = \text{ADC}(\text{Poisson}(\alpha x + \eta)) + \epsilon, \quad (1)$$

where x is the unknown clean image, α is the sensor gain, η is the dark current, and ϵ is the read noise. The inverse problem associated with low-light denoising is to recover x from y . Over the past five decades, the main driving force is to exploit image structures, from Wiener filter [35], total variation [3, 43], wavelets [8] to non-local means [2], BM3D [9], and recently convolution neural networks [1, 5, 17, 24, 48, 55, 61], transformers [34, 37, 60], and diffusion models [25, 58, 66]. A common theme across existing methods is that they all focus on a *generic* prior $p(x)$, i.e., a prior learned from a large collection of example images. While they perform well in moderately difficult problems, the generality of these methods cannot be extended to heavily corrupted images. Particularly in the context of human face recovery, the restored results often lack real identity and exhibit artifacts. This is attributed to the ill-posed nature of the problem and the lack of appropriate constraints.

Why Gallery Photos? Smartphone cameras today store hundreds if not thousands of a user’s photos, captured at different times, in different places, and under different lighting conditions. While these images have many variations, they are all about the *same person(s)*. Therefore, if the imaging goal is to take a photo of this user, the gallery on the phone would be the best source to build a prior $p(x)$. The situation is summarized in Fig. 2. In the context of diffusion-based image restoration, the original solution space can be large because many candidate solutions are consistent with the noisy observation. The gallery provides a strong constraint to the search problem. This allows us to search for better quality images with high precision of the person’s identity.

There are, however, two technical questions:

- What class of images to focus on: In this paper, we will focus on *human faces* because of their relevance to most smartphone users although our algorithm can be equally applied to other image classes. We assume that the gallery photos have been selected and are reasonably informative. Product-level engineering such as pre-processing and selection of the gallery photos is important but beyond the scope of this paper.
- How to incorporate this class-specific $p(x)$ into the restoration model: The bigger (and harder) question is that given the gallery photos, how do we efficiently

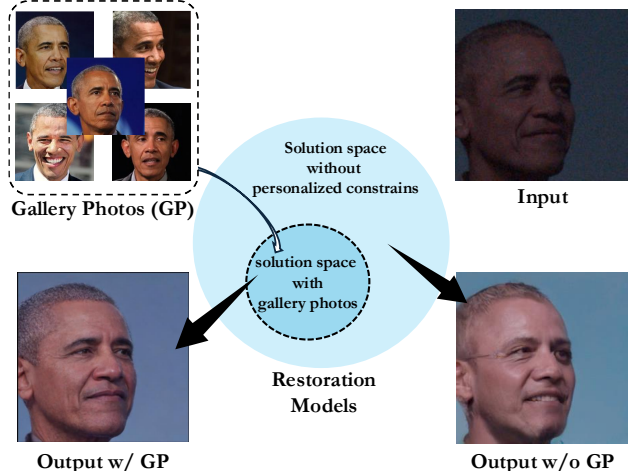


Figure 2. The restoration of inputs degraded by noise and low-light conditions is highly ill-posed. By incorporating additional high-quality gallery photos of the same identity, we significantly reduce the solution space, thereby achieving improved identity consistency in the restored images.

extract the prior information and improve the restoration? We assume that the gallery set is not too big and so we cannot train a restoration model from scratch. We want to avoid fine-tuning as much as possible during inference. Moreover, we want to make sure that the person’s identity is preserved.

Physical Buffers to the Rescue. Given the gallery photos, what kind of prior information would be useful for restoration? Advancements in computer vision have made it possible to extract detailed facial *physical buffers*—including albedo and normal maps—from a person’s gallery of images [42, 63]. These physical buffers capture intrinsic properties such as skin color and surface geometry, effectively encoding an individual’s unique identity and fine facial details. (See Fig. 3.) At the same time, it also eliminates the influence of environmental lighting, pose, and other identity-independent variables. We will leverage this rich prior information to improve restoration.

To convince readers that physical buffers could be useful to our denoising task, we show in Fig. 3 a toy experiment. We consider three types of degradation: low-resolution (LR), motion blur, and noise. In each case, we run an existing physical buffer extraction method DECA [14] to extract the albedo and surface normal of the input. We observe that despite the different types of degradation, the physical buffers (albedo and surface normal) are fairly accurate. The only failure case is when the noise is extremely strong. Therefore, if we can develop solutions to manage the heavy noise case, we will be able to use physical buffers as a signal prior

to guiding the denoising process.

Contributions. Our contributions are threefold:

1. **Personalized Low-Light Denoise and Enhancement Framework:** We introduce a new framework that leverages diffusion models and person-specific priors from photo galleries to address identity loss in restored low-light facial images.
2. **Physical Identity Buffers:** We propose the use of physical identity buffers from existing face galleries to enrich the restoration process, enabling accurate reconstruction of human faces under severe degradation.
3. **Easy Deployment:** Our method operates easily without requiring fine-tuning for individual users, making it practical for real-world applications and scalable to multiple users.

Extensive experiments demonstrate that our approach outperforms existing techniques in both visual quality and identity preservation, providing a significant advancement in low-light facial image restoration.

2. Related Works

Low-light Image Enhancement and Denoising. Low-light images often suffer from significant noise due to low signal-to-noise ratios (SNR), in addition to reduced brightness and contrast. Traditional low-light denoising techniques often focus on exploiting image structures, ranging from early methods like Wiener filtering [35], total variation [3, 43], and wavelets [8] to non-local means [2] and BM3D [9]. More recently, deep learning approaches, including convolutional neural networks [1, 5, 17, 24, 48, 55, 61, 65], transformers [34, 37, 60], and diffusion-based models [25, 41, 58, 66], have emerged as promising solutions for low-light denoising. Low-light image enhancement (LLIE) aims to improve the brightness and contrast of images captured in poorly lit conditions. Traditional approaches [15, 28, 30] often leverage heuristic or physical models to enhance image quality, while learning-based methods [4, 16, 21, 23, 27, 36, 51, 54, 57] have demonstrated greater effectiveness when supported by large-scale datasets. Recent advancements [37, 41, 44, 56] in this field have increasingly focused on jointly addressing denoising and enhancement tasks, aiming to improve image quality while effectively suppressing noise to maintain natural appearance. However, to the best of our knowledge, no specific approach currently exists for joint enhancement and denoising of facial images in low-light conditions.

Deep Face Restoration. CNN/Transformer-based face restoration methods [13, 22, 52], such as RestoreFormer [52], typically rely on paired low- and high-quality image

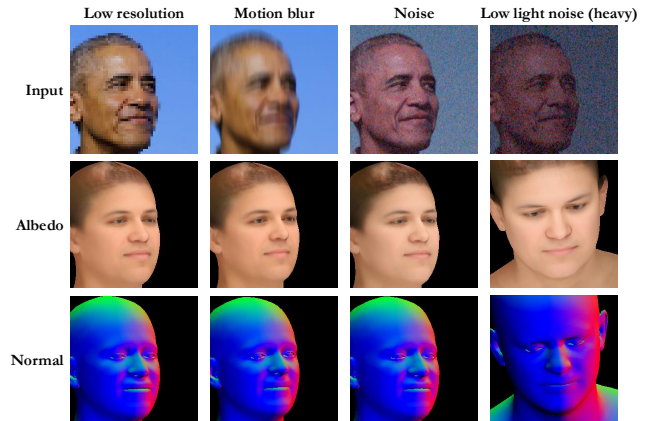


Figure 3. For images affected by mild low resolution, motion blur, or noise, DECA [14] can accurately extract physical buffers. However, DECA fails to obtain precise physical buffers for images degraded by severe low light and noise.

datasets to learn resolution enhancement and noise reduction. While effective, these methods often struggle under severe degradation and lack the capability to synthesize realistic details in complex scenarios.

In recent years, generative priors have been increasingly utilized in face restoration to better address real-world degradations. GAN-based methods, such as GFP-GAN [50], leverage StyleGAN2 [47] to enhance facial details, while diffusion-based models [6, 12, 46, 49, 53] have further expanded restoration capabilities. For instance, BFRDiffusion [6] uses Stable Diffusion to enhance low-quality images by adding high-fidelity details, and Ding *et al.* [12] employ a pretrained diffusion model that denoises degraded inputs while preserving identity by fine-tuning on a person’s gallery photos. MGBFR [46] combines text prompts and reference images with a dual-control adapter to retain accurate facial attributes and identity. Although these generative methods are effective, they often rely on multi-stage training or finetuning, which can limit the efficient use in some real-world applications.

Reference Prior for Face Restoration. In face restoration, reference images [12, 31, 32, 46] provide essential priors for recovering detailed and high-frequency facial features. These priors guide the model to generate realistic restorations. Reference-based methods can be divided into two types: single reference and gallery-based images. The single reference approach [46] uses one image to guide the restoration, focusing on enhancing facial details from a specific reference. In contrast, the gallery-based approach [12] leverages multiple reference images, offering more diverse information and stronger constraints, improving the accuracy and realism of the restoration.

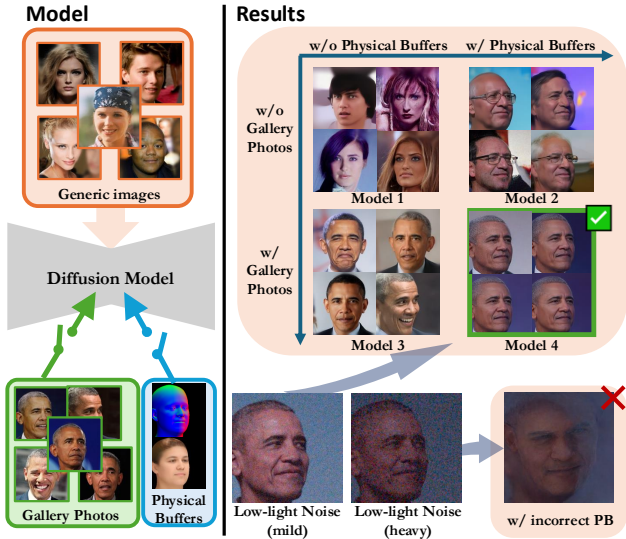


Figure 4. Path to the idea. Using facial physical buffers and gallery images can effectively preserve human face identity information.

3. Method

3.1. Restoration by Diffusion

A diffusion model approximates the clean image distribution $p_\theta(x_0)$ by learning a model θ that reverses the noise-adding process. In Denoising Diffusion Probabilistic Models (DDPMs) [20], Gaussian noise is progressively added to a clean image x_0 :

$$x_t = \sqrt{\alpha_t}x_0 + \sqrt{1 - \alpha_t}\epsilon, \quad \text{where } \epsilon \sim \mathcal{N}(0, I) \quad (2)$$

The reverse process then removes the noise to reconstruct the clean image. After training, for any given time t and the corresponding noisy image x_t , the model can iteratively denoise by sampling from $p(x_0|x_t)$.

In restoration tasks, like low-light denoising, the goal is to recover a high-quality image x_0 from a low-quality input y_0 . Unlike pure generation, where the output can be any image that follows the distribution of clean images, restoration is constrained by the content of y_0 . During training, the model uses y_0 as a condition, and once the model is trained, for any given time t and the corresponding noisy image x_t , it can iteratively denoise by sampling from $p(x_0|x_t, y_0)$ using the trained model.

3.2. Why Gallery + Physical Buffer?

We formalize our core approach of extracting identity-consistent physical buffers from gallery photos to guide the diffusion model for restoration. This method is based on the observation that using facial physical buffers or gallery images can effectively preserve identity information during

restoration tasks involving diffusion models. To evaluate the capability of physical buffers and gallery images in preserving identity information without relying on prior identity knowledge from degraded inputs, we train the following models using a blind scheme, where the degraded input (y_0) is not used as a condition during training. As illustrated in Fig. 4, the models are designed as follows:

- **Model 1:** Trained exclusively on generic images as a purely generative model.
- **Model 2:** Trained on generic images while conditioned on the facial physical buffer extracted from the input image. This model incorporates face identity and facial features through the physical buffer.
- **Model 3:** Fine-tuned on Model 1 with the user’s gallery photos. This model learns identity features from the target person’s gallery photos during fine-tuning.
- **Model 4:** Fine-tuned on Model 2 with the user’s gallery photos. This model integrates facial identity and features from the physical buffer of the input image, as well as the target person’s gallery photos.

We test these models using a simple low-light noisy input. Model 1 generates random faces, as expected for a purely generative model. In contrast, Model 2 produces images with facial features (e.g., nose, mouth, skin color) resembling those of the user. This is because the physical buffers extracted from the degraded user image (refer to Fig. 3) were used as conditioning. These results demonstrate that facial features and identity information can be incorporated by leveraging physical buffers. The outputs from Model 3 are all different user faces, compared to Model 1, showing that fine-tuning with gallery photos can effectively transfer strong identity information. The outputs from Model 4 are the best-expected results, demonstrating the effectiveness of using gallery photos and physical buffers to maintain the person’s identity.

However, despite the powerful combination of gallery images and physical buffer, there are limitations:

- Fine-tuning:** Extracting identity information from gallery photos via fine-tuning is time-consuming and inconvenient. Each time when we switch to a different user, the model must be fine-tuned again. Additionally, since the size of a gallery is usually much smaller than a pre-trained model, fine-tuning can easily overfit.
- Extracting physical buffers from the degraded input image:** If the input is heavily degraded, the physical buffers extracted from it can be wrong (refer to Fig. 3), and result in terrible results as shown in Fig. 4. Besides, the facial feature extracted from a single image

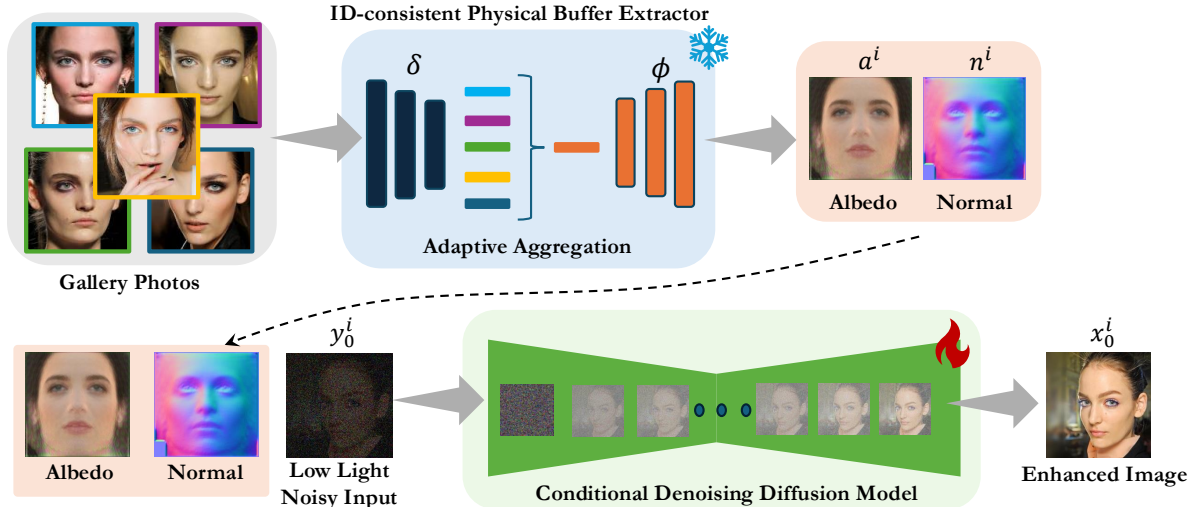


Figure 5. The overall architecture of the proposed method. Our core idea is to use ID-consistent physical buffers, extracted from gallery photos, to constrain the generative space in the diffusion model restoration process. For a high-quality gallery, we use LAP [64] to extract the albedo and normal information for each photo and apply adaptive aggregation to fuse the entire gallery. The extracted albedo represents base skin color and texture details, such as skin tone, freckles, and pigmentation, while normal captures facial geometry, including wrinkles, pores, and fine surface variations. In our framework, the output physical buffers isolate the intrinsic ID properties from lighting, shading, and pose, enabling the diffusion model to apply only ID-related information consistently.

is limited, not to mention from a degraded image.

In conclusion, we want to avoid fine-tuning the model on the gallery and we do not want to extract incorrect physical buffers due to noise.

3.3. ID-Consistent Physical Buffer

To address these limitations, we propose extracting physical buffers directly from existing clean gallery photos and using them as conditions to guide the diffusion model during training. This approach offers significant benefits: clean gallery photos allow us to form comprehensive and robust identity-consistent physical buffers containing detailed facial identity features of the target person. Specifically, We will extract the albedo and normal maps of the target person, which are two key attributes used to describe the physical characteristics of a face.

- **Albedo** captures the intrinsic color of an object’s surface—that is, the subject’s color properties without any lighting effects.
- **Normal** information is used to describe the fine bumps and details such as skin wrinkles and pores.

By conditioning on these strong identity physical buffers, we eliminate the need to fine-tune the model with gallery images and avoid the issue of incorrect buffer extraction. Consequently, the model is better equipped to preserve the target person’s identity and facial features, even under se-

vere degradation.

3.4. Extracting Physical Buffers

Extracting physical buffers for a person from a set of gallery photos is a more challenging task than extracting these buffers from a single input, as in methods like DECA. This complexity arises because gallery photos of the same person are often taken under varying conditions, such as different scenes and poses. To ensure these buffers comprehensively represent the person’s identity and facial details, they must be aligned to maintain identity consistency. Fortunately, existing works have addressed this challenge. As shown in the physical buffer extractor module in Fig. 5, we adopt the aggregation net design from the LAP [64] to extract the ID-consistent physical buffers, which adaptively combines facial features from multiple images to learn consistent geometry and texture representations, and generates ID-consistent albedo and normal maps from a photo collection of the same individual.

3.5. Model Framework

We name our final proposed model **DiffPGD**. As illustrated in Fig. 5, the model leverages ID physical buffers (albedo a^i and normal n^i) extracted from person i ’s gallery photos as conditions to guide our diffusion model during training directs the generative process toward a personalized space.

Within the aggregation network, it contains a shared encoder δ across multiple images and a global decoder ϕ for

predicting consistent face. To model albedo and normal, two separate aggregation networks denoted as (δ^a, ϕ^a) and (δ^n, ϕ^n) , are employed. Given a photo gallery of N images $\{\mathbf{I}_k^i\}_{k=1}^N$ of person i , each image is processed by δ^a and δ^n to extract its texture and geometry latent codes x_k^a and x_k^n , respectively. To derive a global representation of the identity for person i based on $\{x_k^a, x_k^n\}_{k=1}^N$, an adaptive aggregation method is adopted. This method learns a weight set $\{w_k^a, w_k^n\}_{k=1}^N$ according to the quality of each image in $\{\mathbf{I}_k^i\}_{k=1}^N$. The combined global ID-code x_c^a and x_c^n for texture and depth are calculated as:

$$x_c^a = \sum_{k=1}^N w_k^a x_k^a, \quad x_c^n = \sum_{k=1}^N w_k^n x_k^n. \quad (3)$$

Then the global ID-code x_c^a and x_c^n are then passed to the decoders ϕ^a and ϕ^n , respectively, to produce the ID-consistent albedo a^i and normal n^i .

Additionally, with the low-light noisy image y_0^i as another condition during training, other features, such as pose, hairstyle, and background inside the image beyond facial features can be effectively captured as well.

After the model is trained, during testing, the process begins with a Gaussian noise image x_T , which is iteratively transformed into the clean, enhanced image x_0^i by sampling from $p(x_0^i | x_T, y_0^i, a_i, n_i)$ using the trained model. Our experiments demonstrate that identity information is effectively preserved with the guidance of these ID-consistent buffers, enabling our model to achieve superior results in human face restoration.

4. Experiments

4.1. Dataset

Training Data. Since no publicly available datasets exist for low-light noisy face images, we simulate such data using the CelebAMask-HQ dataset [29], the InverseISP algorithm [33], and the Poisson-Gaussian noise model Eq. (1). The pipeline involves converting RGB images to their corresponding RAW mosaiced format using InverseISP [33], followed by applying Eq. (1) to simulate low-light noise using realistic camera sensor parameters. Multiple noise levels are generated by varying the light intensity (Lux) to ensure the model is robust across diverse noise conditions. *Refer to supplementary for more details on the simulation.*

Testing Data. For testing DiffPGD, we utilize both simulated and real-world low-light noisy data. The simulation setup assumes a 12-bit image sensor with parameters similar to that of Canon DSLR cameras: a Full Well Capacity of $36000e^-$, Quantum Efficiency of 0.42, dark current of $7e^-$, and read noise of $6e^-$. These parameters ensure realistic noise characteristics for evaluating model performance. We

collect the real-world test data using the Sony $\alpha 6400$ DSLR camera at an approximate light intensity of 0.13 Lux with an ISO of 25600 and an exposure time of $\frac{1}{8}$ seconds.

4.2. Implementation Details

Our denoising model is built on the ADM architecture [11], and the ID-consistent physical extractor is implemented using the aggregation network from LAP [63]. For training, we use a P2-weighted loss function [7], which measures the discrepancy between the predicted and ground-truth noise. This loss is defined as: $L = \lambda_t \|\hat{\epsilon}_t - \epsilon_t\|_2^2$, where λ_t serves as a hyperparameter to adjust the loss weight dynamically across different timesteps.

During the training stage, we train our model on the CelebAMask-HQ dataset [29], comprising 30,000 images distributed across 4,516 unique identities (IDs). We use 3318 IDs for training and 200 IDs for simulated testing. Within each ID, there are 3–20 images. The Adam optimizer is applied with a learning rate of $1e-4$. Training is performed for 200,000 iterations with a batch size of 32, resulting in a total of 6,400,000 samples seen by the model.

4.3. Performance in Simulated Scenarios

In simulated scenarios, we compare our methods with several state-of-the-art works: UTVNet [65], ACENet [56], GFPGAN [50], SNR-aware [57], DR2 [53], MIRNet [59] and DiffLL [21]. These works aim to restore high-quality images from degraded data that has been affected by low light, noise, or both, which are close to the subject of our research. Particularly, GFPGAN and DR2 are designed specifically for face image restoration, which is highly competitive with our method. We use the 200 test images which correspond to the 200 test IDs from CelebAMask-HQ and send them into our simulator to generate the test set. We simulated five low-light noisy levels by setting different photons per pixel (PPP), which range from 13 PPP to 65 PPP, the lower the PPP, severe the degradation is.

Quantitative and qualitative results are provided. Firstly, we use PSNR, SSIM, and the perceptual metric (LPIPS [62]) to measure the restored image quality. The results are shown in Table 1, it can be seen that our method has surpassed all previous methods by a large scale. Demonstrating the supreme ability of our proposed DiffPGD model on low light denoising and enhancement problems.

Since our work focuses on face images, we also check on the identity preservation performance. Therefore, besides the PSNR, SSIM, and LPIPS metrics, we adopt the identity score which calculates the cosine similarity of the image features extracted by ArcFace [10] to further evaluate the identity consistency. The results are shown in Table 2. Again, our method has the highest identity score. The advantage of our model on preserving the identity is especially



Figure 6. Visual comparison on CelebAMask-HQ test set. Zoom in for the best visual experience.

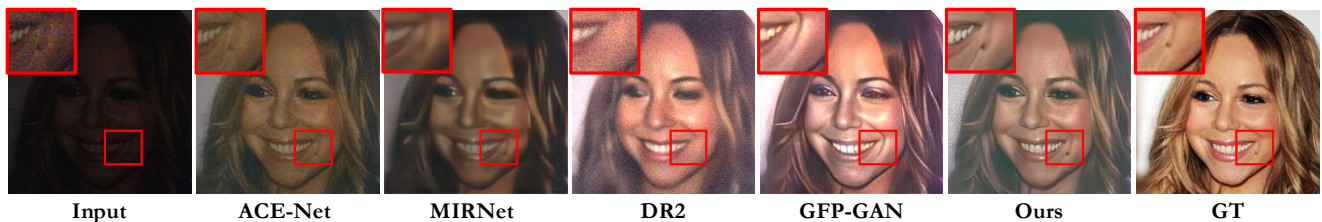


Figure 7. Visual comparison on real-captured photo test (zoomed-in area in the input is scaled for visual purposes). Our method outputs the best denoised and enhanced result, and successfully restores fine facial details, such as moles, wrinkles.

outstanding in heavily degraded cases.

Visualized comparisons are presented in Fig. 6. The image restored from our method has the highest quality and more details, meanwhile preserving the facial identity and maintaining the ID consistent best. Again, the visual results are consistent with the quantitative metric results, the advantage of our model on preserving the identity is especially outstanding in the heavily degraded cases. The sampled gallery photos of the test subject can be found in Fig. 19. Refer to Sec. B in the supplementary material for more visual results.

4.4. Performance in Real-Life Scenarios

Testing model performance in real-life low-light scenarios is crucial, as real-world conditions often involve uncontrol-

lable factors compared to simulated ones. Since no existing dataset addresses the restoration of real-life low-light noisy face photos, we created a custom test set. Specifically, we printed five photos of five target individuals and captured images of these photos under low-light conditions using a camera with the settings specified in Section 4.1. As shown in Fig. 7, our model demonstrates significantly better recovery of real-captured low-light noisy inputs compared to existing models. In Table 3, we quantitatively compare the performance of our model with other baselines on this real-captured photo test. We observe that all our metrics are better except for GFPGAN’s PSNR. However, when looking at the visual comparison in Fig. 7, we realize that GFPGAN recovers smoother features but loses the true facial details, resulting in a relatively fake-looking face. For fur-

Photons Per Pixel	13			26			39			52			65		
Methods	PSNR \uparrow	SSIM \uparrow	LPIPS \downarrow	PSNR \uparrow	SSIM \uparrow	LPIPS \downarrow	PSNR \uparrow	SSIM \uparrow	LPIPS \downarrow	PSNR \uparrow	SSIM \uparrow	LPIPS \downarrow	PSNR \uparrow	SSIM \uparrow	LPIPS \downarrow
UTVNet [65]	12.08	0.2644	0.7816	13.26	0.3685	0.7169	13.99	0.4332	0.6754	14.50	0.4783	0.6419	14.87	0.5118	0.6148
ACENet [56]	11.25	0.2815	0.7431	12.27	0.4022	0.6725	13.19	0.4670	0.6276	13.87	0.5120	0.5894	14.43	0.5479	0.5577
SNR-aware [57]	10.74	0.1186	0.8193	11.99	0.2031	0.7650	12.34	0.2546	0.7230	12.53	0.2935	0.6852	12.76	0.3271	0.6507
MIRNet [59]	11.64	0.4553	0.7476	13.64	0.5416	0.6491	13.90	0.5724	0.5874	14.12	0.5960	0.5355	14.323	0.6154	0.4934
DiffLL [21]	13.30	0.3472	0.7872	14.66	0.4282	0.7189	15.47	0.4588	0.6736	15.96	0.4805	0.6387	16.25	0.4969	0.6072
DR2 [53]	13.50	0.3448	0.7573	15.16	0.5141	0.6430	16.22	0.5655	0.5871	16.85	0.5909	0.5503	17.54	0.6209	0.5181
GFPGAN [50]	13.53	0.4256	0.7049	15.56	0.5446	0.5713	16.60	0.5960	0.5156	17.41	0.6322	0.4748	17.79	0.6563	0.4431
Ours	21.10	0.6287	0.3862	22.80	0.6914	0.3394	23.85	0.7195	0.3156	24.11	0.7354	0.2965	24.38	0.7399	0.2947

Table 1. Quantitative comparison with state-of-the-art works on CelebAMask-HQ dataset.

Methods	13 PPP	26 PPP	39 PPP	52 PPP	65 PPP
UTVNet [65]	0.1572	0.3654	0.5201	0.6197	0.6938
ACENet [56]	0.1734	0.4173	0.5769	0.6756	0.7240
SNR-aware [57]	0.1069	0.1921	0.3114	0.4171	0.4971
MIRNet [59]	0.3071	0.5613	0.6694	0.7246	0.7794
DiffLL [21]	0.1751	0.3779	0.5033	0.6107	0.6682
DR2 [53]	0.2456	0.5128	0.6358	0.6905	0.7239
GFPGAN [50]	0.2506	0.5392	0.6569	0.7212	0.7615
Ours	0.5995	0.7271	0.7702	0.8044	0.8253

Table 2. Comparisons of identity score with other methods on CelebAMask-HQ dataset.

Methods	PSNR \uparrow	SSIM \uparrow	LPIPS \downarrow	ID Score \uparrow
UTVNet [65]	12.02	0.3901	0.6954	0.8062
ACENet [56]	11.36	0.3962	0.6817	0.8125
SNR-aware [57]	10.18	0.1922	0.7274	0.6111
MIRNet [59]	12.48	0.4315	0.7132	0.6914
DiffLL [21]	13.18	0.3899	0.7551	0.7686
DR2 [53]	14.08	0.1829	0.7350	0.5309
GFPGAN [50]	14.18	0.3714	0.6784	0.7138
Ours	14.02	0.4362	0.5954	0.8248

Table 3. Comparisons with state-of-the-art works on real-captured photo test.

Methods	PSNR \uparrow	SSIM \uparrow	LPIPS \downarrow	ID Score \uparrow
w/o physical buffers	12.96	0.3801	0.6196	0.7538
w/ physical buffers	14.02	0.4362	0.5954	0.8248

Table 4. Ablation comparisons of using ID physical buffers on real-captured photo test.

ther verification, we also photographed real individuals under low-light conditions with the camera. As shown in Fig. 8, DiffPGD outperforms existing methods by a large margin. These results confirm that DiffPGD effectively leverages prior information from a target person’s gallery photos to guide the diffusion model in learning a personalized generative space. During restoration, the model accurately directs the output toward this clean personalized space. The gallery photos of the real-captured male subject are displayed in Fig. 9. Other test subjects’ gallery photos can be found in Fig. 19.

5. Ablation Study

ID-Consistent Physical Buffers for Identity Preservation. We have shown that the proposed model DiffPGD exhibits outstanding performance in both simulated and real-world testing scenarios. In Table 4, we compare the quantitative results of training our model with and without ID physical buffers in real-world test cases. The results demonstrate that using physical buffers largely increases the identity score, highlighting the effectiveness of extracting ID physical buffers from a person’s existing photo gallery to assist in restoring real-world low-quality photos.

6. Conclusion

In this work, we addressed the challenges of low-light image restoration by introducing Personalized Generative Denoising (PGD), a novel approach that leverages user-specific photo galleries to improve denoising performance. By incorporating an identity-consistent physical buffer, we provided a strong prior that enhances the diffusion model’s ability to restore degraded images while avoiding the need for model fine-tuning. Our experiments demonstrated that PGD outperforms existing diffusion-based denoising methods, delivering superior results across various testing scenarios. This approach not only mitigates false content generation in low-SNR conditions but also bridges the gap in low-light imaging quality, paving the way for personalized and more robust image restoration techniques.

Acknowledgment This research was supported, in part, by a research contract from Samsung Research America, the National Science Foundation (NSF), and in part by the Intelligence Advanced Research Projects Activity (IARPA) under Contract No. 2022-21102100004, and in part by the National Science Foundation under the grants CCSS-2030570 and IIS-2133032. The views and conclusions contained herein are those of the authors and should not be interpreted as necessarily representing the official policies, either expressed or implied, of IARPA, or the U.S. Government. The U.S. Government is authorized to reproduce and distribute reprints for governmental purposes notwithstanding any copyright annotation therein.

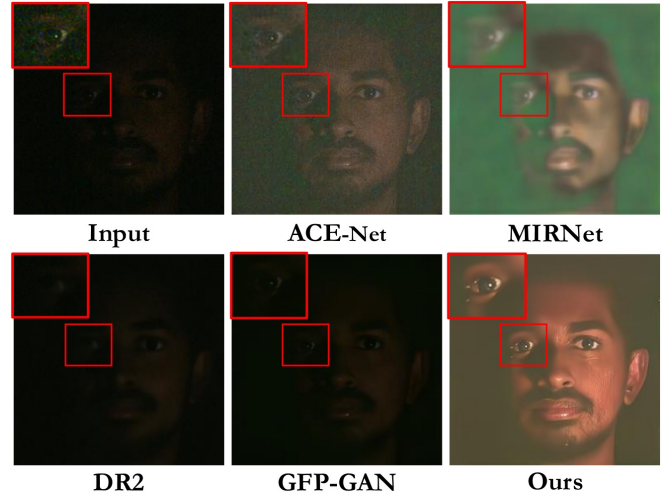


Figure 8. (Left) Environmental setup, real-life low-light noisy photo taken in the dark room. (Right) Visual comparison on the real-world captured SUBJECT.



Figure 9. Male SUBJECT's gallery (face areas are cropped from the subject's photos).

References

- [1] Tim Brooks, Ben Mildenhall, Tianfan Xue, Jiawen Chen, Dillon Sharlet, and Jonathan T. Barron. Unprocessing images for learned raw denoising. In *IEEE/CVF Conference on Computer Vision and Pattern Recognition*, pages 11028–11037, 2019. [2](#), [3](#)
- [2] A. Buades, B. Coll, and J.-M. Morel. A non-local algorithm for image denoising. In *IEEE Conference on Computer Vision and Pattern Recognition*, volume 2, pages 60–65, 2005. [2](#), [3](#)
- [3] A Chambolle. An algorithm for total variation minimization and applications. *Journal of Mathematical Imaging and Vision*, 20:89–97, 2004. [2](#), [3](#)
- [4] Chen Chen, Qifeng Chen, Jia Xu, and Vladlen Koltun. Learning to see in the dark. In *IEEE/CVF Conference on Computer Vision and Pattern Recognition*, pages 3291–3300, 2018. [3](#)
- [5] Jingwen Chen, Jiawei Chen, Hongyang Chao, and Ming Yang. Image blind denoising with generative adversarial network based noise modeling. In *IEEE/CVF Conference on Computer Vision and Pattern Recognition*, pages 3155–3164, 2018. [2](#), [3](#)
- [6] Xiaoxu Chen, Jingfan Tan, Tao Wang, Kaihao Zhang, Wenhan Luo, and Xiaochun Cao. Toward real-world blind face restoration with generative diffusion prior. *IEEE Transactions on Circuits and Systems for Video Technology*, 34(9):8494–8508, 2024. [3](#)
- [7] Jooyoung Choi, Jungbeom Lee, Chaehun Shin, Sungwon Kim, Hyunwoo Kim, and Sungroh Yoon. Perception prioritized training of diffusion models. In *IEEE/CVF Conference on Computer Vision and Pattern Recognition*, pages 11472–11481, 2022. [6](#)
- [8] R. R. Coifman and D. L. Donoho. *Translation-Invariant Denoising*, pages 125–150. 1995. [2](#), [3](#)
- [9] Kostadin Dabov, Alessandro Foi, Vladimir Katkovnik, and Karen Egiazarian. Image denoising by sparse 3-d transform-domain collaborative filtering. *IEEE Transactions on Image Processing*, 16(8):2080–2095, 2007. [2](#), [3](#)
- [10] Jiankang Deng, Jia Guo, Niannan Xue, and Stefanos Zafeiriou. Arcface: Additive angular margin loss for deep face recognition. In *IEEE/CVF conference on computer vision and pattern recognition*, pages 4690–4699, 2019. [6](#)

- [11] Prafulla Dhariwal and Alexander Nichol. Diffusion models beat gans on image synthesis. *Advances in neural information processing systems*, 34:8780–8794, 2021. 6, 14
- [12] Zheng Ding, Xuaner Zhang, Zhuowen Tu, and Zhihao Xia. Restoration by generation with constrained priors. In *IEEE/CVF Conference on Computer Vision and Pattern Recognition*, 2024. 3
- [13] Yingruo Fan, Zhaojiang Lin, Jun Saito, Wenping Wang, and Taku Komura. Faceformer: Speech-driven 3d facial animation with transformers. In *IEEE/CVF Conference on Computer Vision and Pattern Recognition*, 2022. 3
- [14] Yao Feng, Haiwen Feng, Michael J Black, and Timo Bolkart. Learning an animatable detailed 3d face model from in-the-wild images. *ACM Transactions on Graphics*, 40(4):1–13, 2021. 2, 3
- [15] Xueyang Fu, Delu Zeng, Yue Huang, Xiao-Ping Zhang, and Xinghao Ding. A weighted variational model for simultaneous reflectance and illumination estimation. In *IEEE Conference on Computer Vision and Pattern Recognition*, pages 2782–2790, 2016. 3
- [16] Chunle Guo, Chongyi Li, Jichang Guo, Chen Change Loy, Junhui Hou, Sam Kwong, and Runmin Cong. Zero-reference deep curve estimation for low-light image enhancement. In *IEEE/CVF Conference on Computer Vision and Pattern Recognition*, pages 1777–1786, 2020. 3
- [17] Shi Guo, Zifei Yan, Kai Zhang, Wangmeng Zuo, and Lei Zhang. Toward convolutional blind denoising of real photographs. In *IEEE/CVF Conference on Computer Vision and Pattern Recognition*, pages 1712–1722, 2019. 2, 3
- [18] Kaiming He, Xiangyu Zhang, Shaoqing Ren, and Jian Sun. Deep residual learning for image recognition. In *Proceedings of the IEEE conference on computer vision and pattern recognition*, pages 770–778, 2016. 14
- [19] Martin Heusel, Hubert Ramsauer, Thomas Unterthiner, Bernhard Nessler, and Sepp Hochreiter. Gans trained by a two time-scale update rule converge to a local nash equilibrium. In *Advances in Neural Information Processing Systems*, pages 6626–6637, 2017. 13
- [20] Jonathan Ho, Ajay Jain, and Pieter Abbeel. Denoising diffusion probabilistic models. In *Advances in Neural Information Processing Systems*, page 6840–6851, 2020. 4
- [21] Hai Jiang, Ao Luo, Haoqiang Fan, Songchen Han, and Shuaicheng Liu. Low-light image enhancement with wavelet-based diffusion models. *ACM Transactions on Graphics*, 42(6):1–14, 2023. 3, 6, 8, 13
- [22] Kui Jiang, Zhongyuan Wang, Peng Yi, Tao Lu, Junjun Jiang, and Zixiang Xiong. Dual-path deep fusion network for face image hallucination. *IEEE Transactions on Neural Networks and Learning Systems*, 33(1):378–391, 2022. 3
- [23] Yifan Jiang, Xinyu Gong, Ding Liu, Yu Cheng, Chen Fang, Xiaohui Shen, Jianchao Yang, Pan Zhou, and Zhangyang Wang. Enlightengan: Deep light enhancement without paired supervision. *IEEE Transactions on Image Processing*, 30:2340–2349, 2021. 3
- [24] Kyong Hwan Jin, Michael T. McCann, Emmanuel Froustey, and Michael Unser. Deep convolutional neural network for inverse problems in imaging. *IEEE Transactions on Image Processing*, 26(9):4509–4522, 2017. 2, 3
- [25] Bahjat Kawar, Michael Elad, Stefano Ermon, and Jiaming Song. Denoising diffusion restoration models. In *Advances in Neural Information Processing Systems*, 2022. 2, 3
- [26] Diederik P Kingma. Adam: A method for stochastic optimization. *arXiv preprint arXiv:1412.6980*, 2014. 14
- [27] Edwin H Land and John J McCann. Lightness and retinex theory. *JOSA*, 1971. 3
- [28] Chulwoo Lee, Chul Lee, and Chang-Su Kim. Contrast enhancement based on layered difference representation of 2d histograms. *IEEE Transactions on Image Processing*, 22(12):5372–5384, 2013. 3
- [29] Cheng-Han Lee, Ziwei Liu, Lingyun Wu, and Ping Luo. Maskgan: Towards diverse and interactive facial image manipulation. In *IEEE Conference on Computer Vision and Pattern Recognition (CVPR)*, 2020. 6, 12
- [30] Mading Li, Jiaying Liu, Wenhan Yang, Xiaoyan Sun, and Zongming Guo. Structure-revealing low-light image enhancement via robust retinex model. *IEEE Transactions on Image Processing*, 27(6):2828–2841, 2018. 3
- [31] Xiaoming Li, Wenyu Li, Dongwei Ren, Hongzhi Zhang, Meng Wang, and Wangmeng Zuo. Enhanced blind face restoration with multi-exemplar images and adaptive spatial feature fusion. In *IEEE/CVF Conference on Computer Vision and Pattern Recognition*, 2020. 3
- [32] Xiaoming Li, Shiguang Zhang, Shangchen Zhou, Lei Zhang, and Wangmeng Zuo. Learning dual memory dictionaries for blind face restoration. *IEEE Transactions on Pattern Analysis and Machine Intelligence*, 2022. 3
- [33] Zhihao Li, Ming Lu, Xu Zhang, Xin Feng, M Salman Asif, and Zhan Ma. Efficient visual computing with camera raw snapshots. *IEEE Transactions on Pattern Analysis and Machine Intelligence*, 2024. 6, 12
- [34] Jingyun Liang, Jie Zhang Cao, Guolei Sun, Kai Zhang, Luc Van Gool, and Radu Timofte. Swinir: Image restoration using swin transformer. In *IEEE/CVF International Conference on Computer Vision Workshops*, pages 1833–1844, 2021. 2, 3
- [35] Jae S. Lim. Two-dimensional signal and image processing. 1989. 2, 3
- [36] Kun Lu and Lihong Zhang. Tbefn: A two-branch exposure-fusion network for low-light image enhancement. *IEEE Transactions on Multimedia*, 23:4093–4105, 2021. 3
- [37] Yucheng Lu and Seung-Won Jung. Progressive joint low-light enhancement and noise removal for raw images. *IEEE Transactions on Image Processing*, 31:2390–2404, 2022. 2, 3
- [38] Jiaju Ma, Stanley Chan, and Eric R. Fossum. Review of quanta image sensors for ultralow-light imaging. *IEEE Transactions on Electron Devices*, 69(6):2824–2839, 2022. 1
- [39] Jiaju Ma and Eric R. Fossum. A pump-gate jot device with high conversion gain for a quanta image sensor. *IEEE Journal of the Electron Devices Society*, 3(2):73–77, 2015. 1
- [40] Junichi Nakamura. *Image Sensors and Signal Processing for Digital Still Cameras*. CRC Press, 2006. 1
- [41] Cindy M Nguyen, Eric R Chan, Alexander W Bergman, and Gordon Wetzstein. Diffusion in the dark: A diffusion model

- for low-light text recognition. In *IEEE/CVF Winter Conference on Applications of Computer Vision*, 2024. 3
- [42] Joseph Roth, Yiying Tong, and Xiaoming Liu. Adaptive 3d face reconstruction from unconstrained photo collections. In *IEEE/CVF conference on computer vision and pattern recognition*, pages 4197–4206, 2016. 2
- [43] L.I. Rudin and S. Osher. Total variation based image restoration with free local constraints. In *International Conference on Image Processing*, volume 1, pages 31–35, 1994. 2, 3
- [44] Yiqi Shi, Duo Liu, Liguang Zhang, Ye Tian, Xuezhi Xia, and Xiaojing Fu. Zero-ig: Zero-shot illumination-guided joint denoising and adaptive enhancement for low-light images. In *IEEE/CVF Conference on Computer Vision and Pattern Recognition*, pages 3015–3024, 2024. 3
- [45] Jiaming Song, Chenlin Meng, and Stefano Ermon. Denoising diffusion implicit models. *arXiv preprint arXiv:2010.02502*, 2020. 14
- [46] Keda Tao, Jinjin Gu, Yulun Zhang, Xiucheng Wang, and Nan Cheng. Overcoming false illusions in real-world face restoration with multi-modal guided diffusion model. *arXiv preprint arXiv: 2410.04161*, 2024. 3
- [47] Omer Tov, Yuval Alaluf, Yotam Nitzan, Or Patashnik, and Daniel Cohen-Or. Designing an encoder for stylegan image manipulation. *ACM Trans. Graph.*, 40(4), 2021. 3
- [48] Subarna Tripathi, Zachary C. Lipton, and Truong Q. Nguyen. Correction by projection: Denoising images with generative adversarial networks, 2018. 2, 3
- [49] Tuomas Varanka, Tapani Toivonen, Soumya Tripathy, Guoying Zhao, and Erman Acar. Pfstorer: Personalized face restoration and super-resolution. In *IEEE/CVF Conference on Computer Vision and Pattern Recognition*, pages 2372–2381, 2024. 3, 14
- [50] Xintao Wang, Yu Li, Honglun Zhang, and Ying Shan. Towards real-world blind face restoration with generative facial prior. In *IEEE/CVF conference on computer vision and pattern recognition*, pages 9168–9178, 2021. 1, 3, 6, 8, 13
- [51] Yufei Wang, Yi Yu, Wenhan Yang, Lanqing Guo, Lap-Pui Chau, Alex C Kot, and Bihan Wen. Exposediffusion: Learning to expose for low-light image enhancement. In *IEEE International Conference on Computer Vision*, 2023. 3
- [52] Zhouxia Wang, Jiawei Zhang, Runjian Chen, Wenping Wang, and Ping Luo. Restoreformer: High-quality blind face restoration from undegraded key-value pairs. In *IEEE/CVF Conference on Computer Vision and Pattern Recognition*, pages 17491–17500, 2022. 3
- [53] Zhixin Wang, Ziyang Zhang, Xiaoyun Zhang, Huangjie Zheng, Mingyuan Zhou, Ya Zhang, and Yanfeng Wang. Dr2: Diffusion-based robust degradation remover for blind face restoration. In *IEEE/CVF Conference on Computer Vision and Pattern Recognition*, pages 1704–1713, 2023. 1, 3, 6, 8, 13
- [54] Chen Wei, Wenjing Wang, Wenhan Yang, and Jiaying Liu. Deep retinex decomposition for low-light enhancement. In *British Machine Vision Conference*, 2018. 3
- [55] Kaixuan Wei, Ying Fu, Jiaolong Yang, and Hua Huang. A physics-based noise formation model for extreme low-light raw denoising. In *IEEE/CVF Conference on Computer Vision and Pattern Recognition*, 2020. 2, 3
- [56] Ke Xu, Xin Yang, Baocai Yin, and Rynson WH Lau. Learning to restore low-light images via decomposition-and-enhancement. In *IEEE/CVF conference on computer vision and pattern recognition*, pages 2281–2290, 2020. 3, 6, 8, 13
- [57] Xiaogang Xu, Ruixing Wang, Chi-Wing Fu, and Jiaya Jia. Snr-aware low-light image enhancement. In *IEEE/CVF conference on computer vision and pattern recognition*, pages 17714–17724, 2022. 3, 6, 8, 13
- [58] Cheng Yang, Lijing Liang, and Zhixun Su. Real-world denoising via diffusion model, 2023. 2, 3
- [59] Syed Waqas Zamir, Aditya Arora, Salman Khan, Munawar Hayat, Fahad Shahbaz Khan, Ming-Hsuan Yang, and Ling Shao. Learning enriched features for real image restoration and enhancement. In *European Conference on Computer Vision*, pages 492–511. Springer, 2020. 6, 8, 13
- [60] Jiale Zhang, Yulun Zhang, Jinjin Gu, Jiahua Dong, Linghe Kong, and Xiaokang Yang. Xformer: Hybrid x-shaped transformer for image denoising. In *International Conference on Learning Representations*, 2024. 2, 3
- [61] Kai Zhang, Wangmeng Zuo, Yunjin Chen, Deyu Meng, and Lei Zhang. Beyond a gaussian denoiser: Residual learning of deep cnn for image denoising. *IEEE Transactions on Image Processing*, 26(7):3142–3155, 2017. 2, 3
- [62] Richard Zhang, Phillip Isola, Alexei A Efros, Eli Shechtman, and Oliver Wang. The unreasonable effectiveness of deep features as a perceptual metric. In *IEEE conference on computer vision and pattern recognition*, pages 586–595, 2018. 6
- [63] Zhenyu Zhang, Yanhao Ge, Renwang Chen, Ying Tai, Yan Yan, Jian Yang, Chengjie Wang, Jilin Li, and Feiyue Huang. Learning to aggregate and personalize 3d face from in-the-wild photo collection. In *IEEE/CVF Conference on Computer Vision and Pattern Recognition*, pages 14214–14224, 2021. 2, 6
- [64] Zhenyu Zhang, Yanhao Ge, Renwang Chen, Ying Tai, Yan Yan, Jian Yang, Chengjie Wang, Jilin Li, and Feiyue Huang. Learning to aggregate and personalize 3d face from in-the-wild photo collection. In *IEEE/CVF Conference on Computer Vision and Pattern Recognition*, pages 14214–14224, 2021. 5
- [65] Chuanjun Zheng, Daming Shi, and Wentian Shi. Adaptive unfolding total variation network for low-light image enhancement. In *IEEE/CVF international conference on computer vision*, pages 4439–4448, 2021. 3, 6, 8, 13
- [66] Yuanzhi Zhu, Kai Zhang, Jingyun Liang, Jie Zhang Cao, Bihan Wen, Radu Timofte, and Luc Van Gool. Denoising diffusion models for plug-and-play image restoration. In *IEEE Conference on Computer Vision and Pattern Recognition Workshops (NTIRE)*, 2023. 2, 3

Supplementary Material

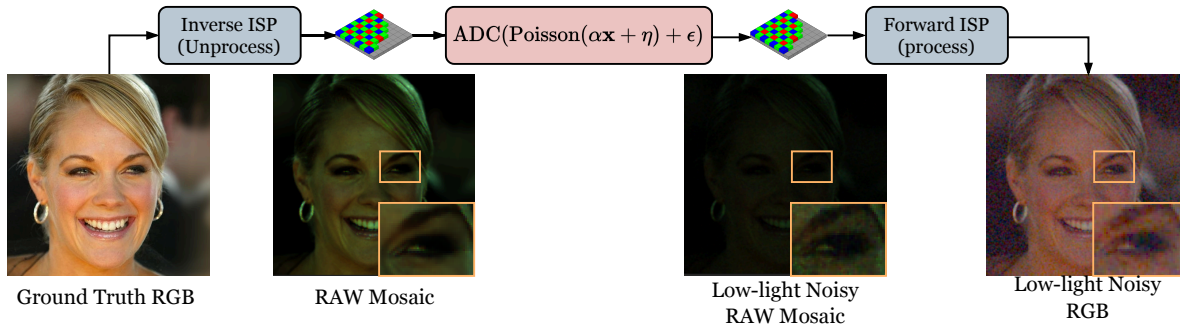


Figure 9. Simulation process for generating low-light noisy face images.

A. Dataset

As mentioned in Section 4.1 of the main paper, since no open-sourced low-light noisy datasets are available, we adopt a simulation approach to generate low-light noisy face images for training our model. Specifically, we utilize the CelebAMask-HQ dataset’s [29] face images as the ground truth RGB images.

As shown in Fig. 9, the first step in the simulation process involves passing the RGB image through a pre-trained Inverse ISP network [33] to generate a pseudo ground truth RAW mosaic image. For visualization purposes, we display the demosaiced version of this image. We utilize the pretrained weights provided by the authors [33], which were obtained by training the network on iPhone camera images, for unprocessing the RGB images into RAW format.

This pseudo ground truth RAW image is then passed through a Poisson-Gaussian Simulator to simulate the low-light noisy RAW mosaic image. It is noteworthy that during the training process, we vary the camera sensor parameters (in the Poisson-Gaussian simulator) across a wide range of values to enable the model to handle diverse camera sensor noise profiles. The simulation setup assumes a 12-bit image sensor with parameters similar to those of Canon DSLR cameras. The parameter ranges are summarized in Table 5.

Parameter	Range
Full Well Capacity	$[19000e^-, 64000e^-]$
Quantum Efficiency	$[0.32, 0.54]$
Dark Current	$[2.2e^-, 11.7e^-]$
Read Noise	$[2.2e^-, 10.8e^-]$
Photons-per-Pixel (PPP)	$[13 \text{ PPP}, 65 \text{ PPP}]$

Table 5. Simulation parameters used in the Poisson-Gaussian Simulator.

These parameters are carefully chosen to ensure realistic noise characteristics during training.

B. Additional Visual Results

In Fig. 16, Fig. 17 and Fig. 18, we present additional visual comparisons between our model and baseline methods. Our results consistently demonstrate superior performance, particularly in cases of severe degradation.

C. Results in More Severe Cases

To further evaluate the ability of our model to denoise and enhance extremely degraded photos, we tested it under highly challenging conditions, including both simulated and real-life scenarios.

For simulated cases, We simulate severely degraded test cases with 10 PPP and 5 PPP. As shown in Fig. 12 and Fig. 13, our model can still perform well in terms of enhancing and denoising the degraded inputs, whereas other models struggled significantly. Besides, due to the extremely low signal level in the input image, we can see some hallucination effect in the hairstyle of the generated outputs. Despite this, thanks to the ID physical buffer extracted from the gallery of the target person, our model could still effectively restore the facial structure of the target person. Quantitative comparisons are presented in Tables 7 and 8.

We also evaluated the model on real-captured photos. Fig. 14 is a visual example of the male subject taken under extremely low light conditions with high noise levels. From the figure, we can see that our proposed model outperforms all baseline methods in both denoising and enhancement. Additionally, the blind-based restoration methods DR2 and GFPGAN completely failed to produce meaningful results due to the severely low signal levels. This supports our observation that blind restoration approaches struggle with

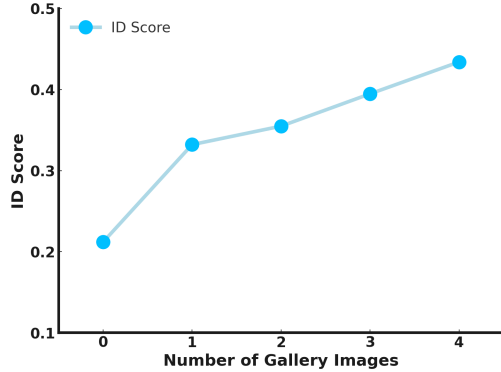


Figure 10. The relationship between the identity (ID) score of the restored images and the number of gallery images used to generate the ID physical buffer.

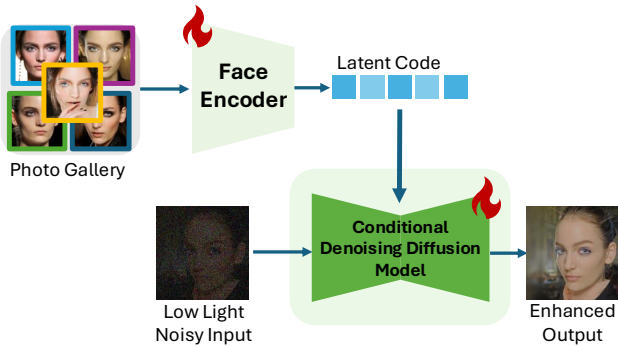


Figure 11. A network architecture diagram for identity feature restoration using a face encoder.

images degraded by extremely low light and noise. For these real-captured extreme test cases, we further conducted quantitative evaluations of both image quality and identity preservation, as summarized in Table 6. Since ground truth images are unavailable for real-captured cases, we computed the Fréchet Inception Distance (FID) [19] between the model’s output images and the subject’s gallery photos, which are 4 clean natural photos from the subject’s phone (shown in Fig. 9). We calculate the identity (ID) score by averaging the ID scores between the model’s output images and each gallery photo. The results indicate that our model consistently achieves superior image quality and identity preservation compared to other methods.

D. More Ablation Study

The proposed DiffPGD model is conditioned with the ID physical buffers extracted from the User’s gallery photos. As claimed in the paper, facial features extracted from a single image are inherently limited. In Fig. 10, we evaluate the effect of the number of gallery images used to gener-

Methods	FID ↓	ID Score ↑
UTVNet [65]	293.2	0.31
ACENet [56]	338.5	0.13
MIRNet [59]	387.7	0.13
DiffLL [21]	355.1	0.36
DR2 [53]	341.0	0.06
GFPGAN [50]	316.8	0.06
Ours	284.2	0.43

Table 6. Comparisons with state-of-the-art works on the real-captured test cases under extreme conditions.

Photons Per Pixel	5			10		
	PSNR ↑	SSIM ↑	LPIPS ↓	PSNR ↑	SSIM ↑	LPIPS ↓
UTVNet [65]	11.06	0.1756	0.8275	11.71	0.2226	0.8067
ACENet [56]	9.97	0.1741	0.7949	10.81	0.2326	0.7683
SNR-aware [57]	9.11	0.0590	0.8527	9.91	0.0864	0.8366
MIRNet [59]	9.05	0.3376	0.8546	10.02	0.3896	0.8004
DiffLL [21]	11.96	0.2832	0.8448	12.67	0.3109	0.8143
DR2 [53]	7.17	0.1902	0.7435	8.08	0.2399	0.7437
GFPGAN [50]	7.20	0.2211	0.7251	8.13	0.2845	0.7185
Ours	17.93	0.5375	0.4731	18.49	0.6115	0.4120

Table 7. Quantitative comparison with state-of-the-art works on CelebAMask-HQ dataset under extreme conditions.

Methods	5 PPP	10 PPP
UTVNet [65]	0.0998	0.1129
ACENet [56]	0.0999	0.1233
SNR-aware [57]	0.0988	0.1001
MIRNet [59]	0.0991	0.1747
DiffLL [21]	0.1004	0.1209
DR2 [53]	0.0987	0.1043
GFPGAN [50]	0.0949	0.1176
Ours	0.5995	0.7271

Table 8. Comparisons of identity score with other methods on CelebAMask-HQ dataset under extreme conditions.

Methods	PSNR ↑	SSIM ↑	LPIPS ↓	ID Score ↑
w/ Encoder	12.62	0.2574	0.6315	0.6906
w/ physical buffers	13.85	0.3753	0.6042	0.8039

Table 9. Comparison of ID physical buffers and encoder-based methods on the real-world photo test set. For a fair comparison, we use two same gallery images for each individual for both the encoder-based and physical buffer-based approaches.

ate the ID physical buffer on identity preservation performance. We analyze it with the real-captured extreme test set where 4 gallery images were collected from the subject’s phone. The results show that identity preservation improves as the ID physical buffer is derived from a greater number of gallery photos rather than a single image. Additionally, incorporating the ID physical buffer significantly enhances identity preservation compared to not using it, which corre-

sponds to the case with zero gallery photos.

E. More Implementation Details

During training and testing, the image size is 256×256 . The architecture of the diffusion model is adapted from [11]. We modify the architecture so that the model can take the concatenation of physical buffers and degraded images as conditions. The model parameters are configured as follows: the number of channels is set to 128, channel multiple is (1, 1, 2, 2, 4, 4), head channels are 128, attention resolution is 16, dropout rate is 0.1, diffusion steps are 1000, and the two hyperparameters $P2_gamma$ and $p2_k$ are both set to 1.0. For additional architectural details, refer to [11]. During inference, we adopt the DDIM method [45] with 200 denoising steps. The model is trained using the Adam optimizer [26] with a learning rate of 10^{-4} . The weight decay is set to 0. All experiments are performed on a single NVIDIA A100 GPU.

F. Encoder vs. Physical Buffer?

Many previous studies have used encoder-based methods to extract latent facial feature information from reference photos [49]. To evaluate whether the encoder can effectively extract enough facial features to guide the diffusion model in solving the low-light enhancement and denoising task, we conducted an experiment. As illustrated in Fig. 11, we utilized an encoder (ResNet-18 [18]) to extract latent codes from the target individual’s gallery photos. Following the method employed by ADM [11] for time embedding, we scaled and shifted the features in each layer of the diffusion model using the latent codes. This process integrates the identity information extracted by the encoder into the diffusion model.

We compared the restored images generated with the encoder-based method with the proposed physical buffer-guided method on our real-captured photo set. The quantitative and visual comparisons are presented in Table 9 and Fig. 15, respectively. The results demonstrate that guiding the diffusion model using ID physical buffers produces significantly better identity preservation than the encoder-based approach. One major reason for this is that the ID physical buffers serve as robust conditions, enabling the extraction of comprehensive facial features from the gallery. In contrast, the encoder-based method is less focused on facial features and is often influenced by irrelevant factors such as background and hairstyle. Consequently, the latent codes extracted by the encoder are less effective in guiding the diffusion model to the personalized generative space compared to the ID physical buffers.

G. Gallery Photos

Fig. 19 presents the sampled gallery photos for each test subject included in the main paper and supplementary material. Additionally, the gallery photos of the real-captured male subject are displayed in Fig. 9.

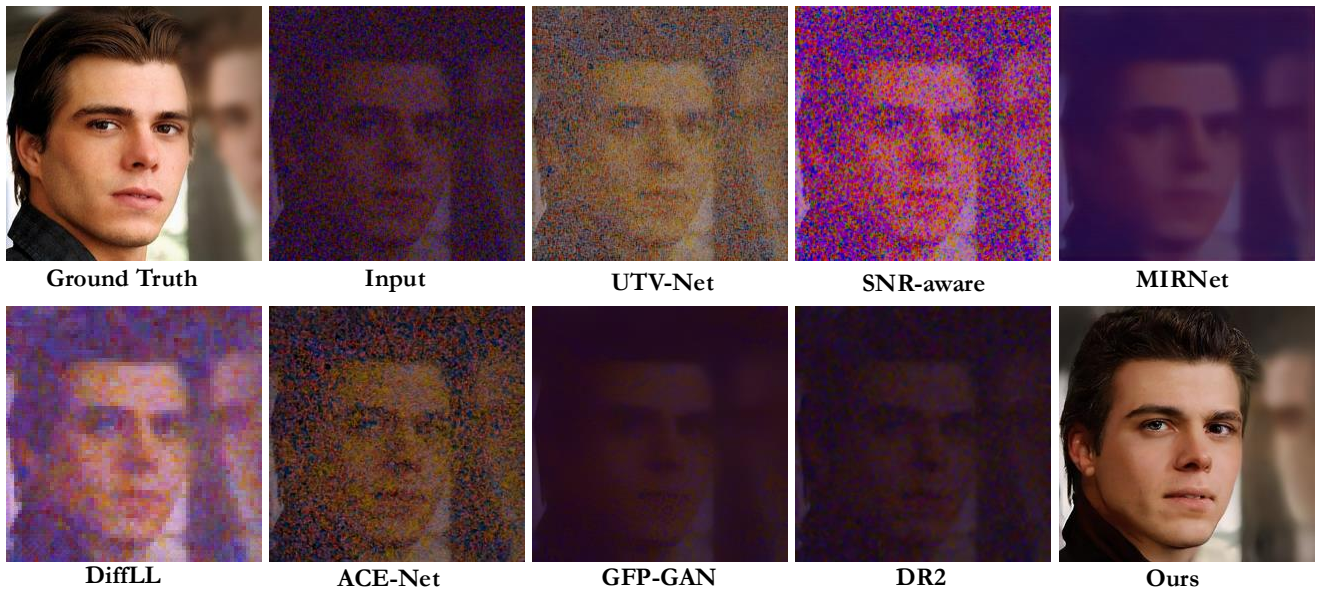


Figure 12. Visual comparison on CelebAMask-HQ test set under extreme conditions (10 PPP).

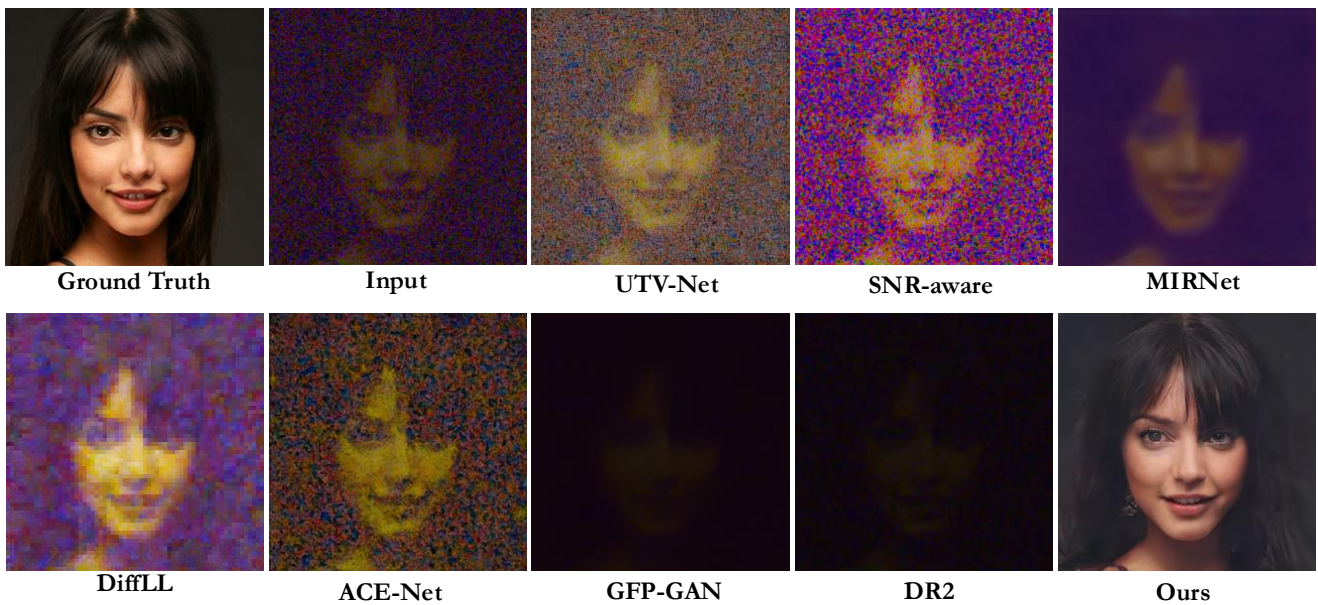


Figure 13. Visual comparison on CelebAMask-HQ test set under extreme conditions (5 PPP).

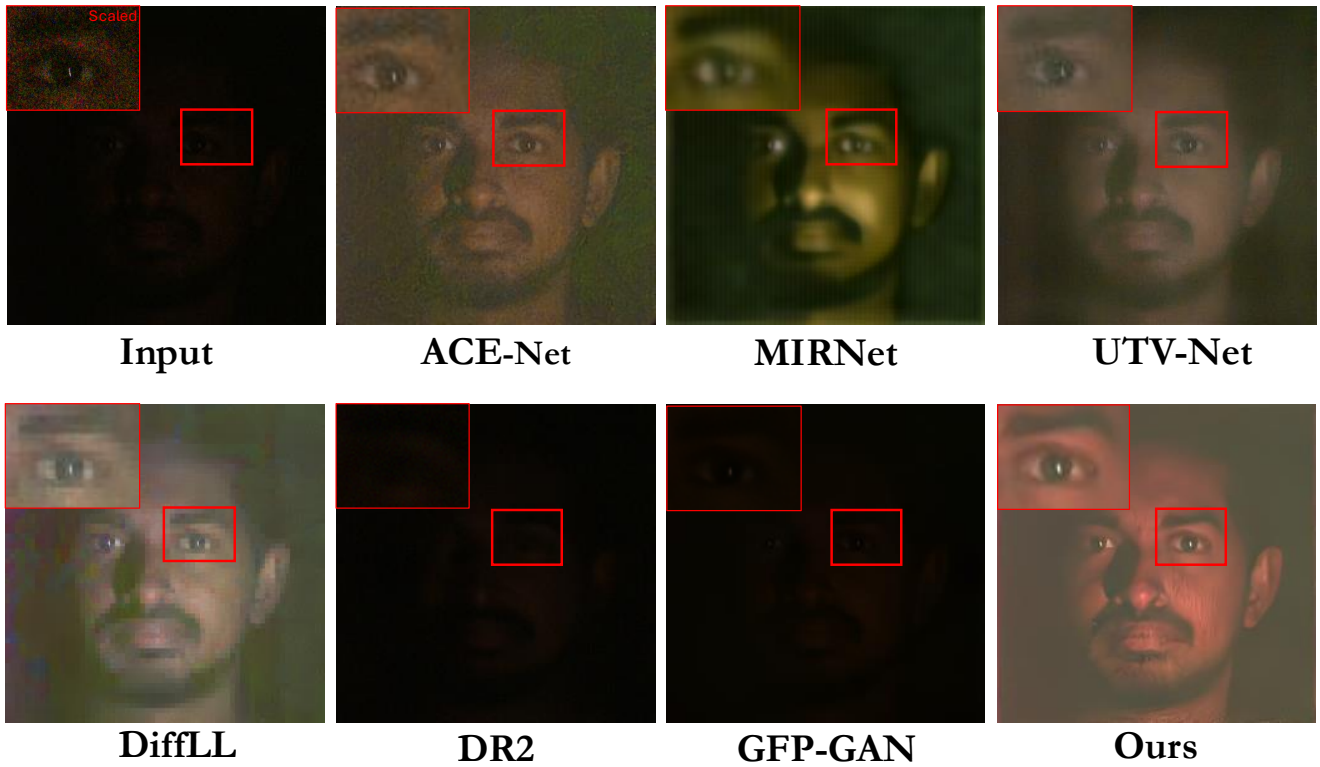


Figure 14. Visual comparison on the real-world captured SUBJECT under extreme conditions (zoomed-in area in the input is scaled for visual purposes).

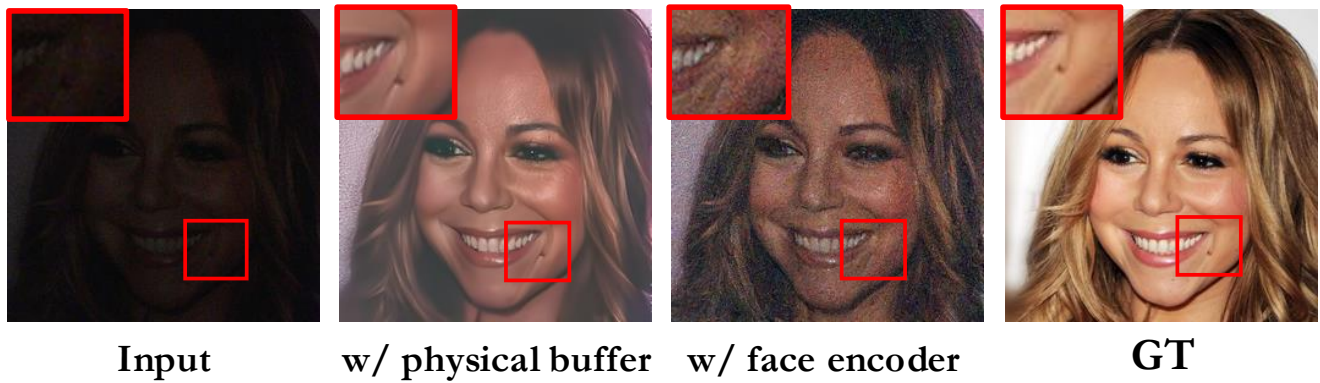


Figure 15. Visual comparison on different identity representation strategies (physical buffer and face encoder).

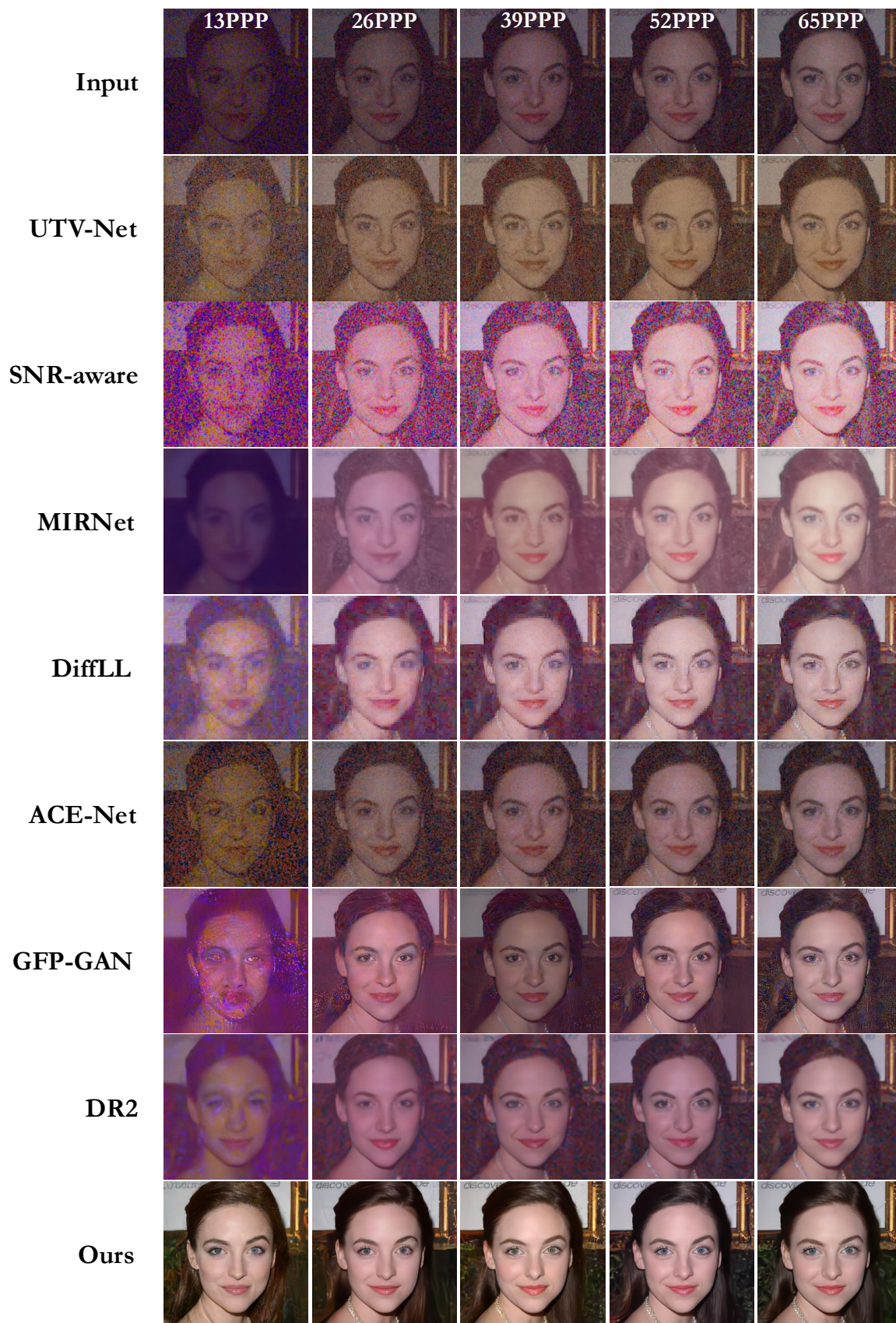


Figure 16. Visual comparison on CelebAMask-HQ test set. Zoom in for the best visual experience.

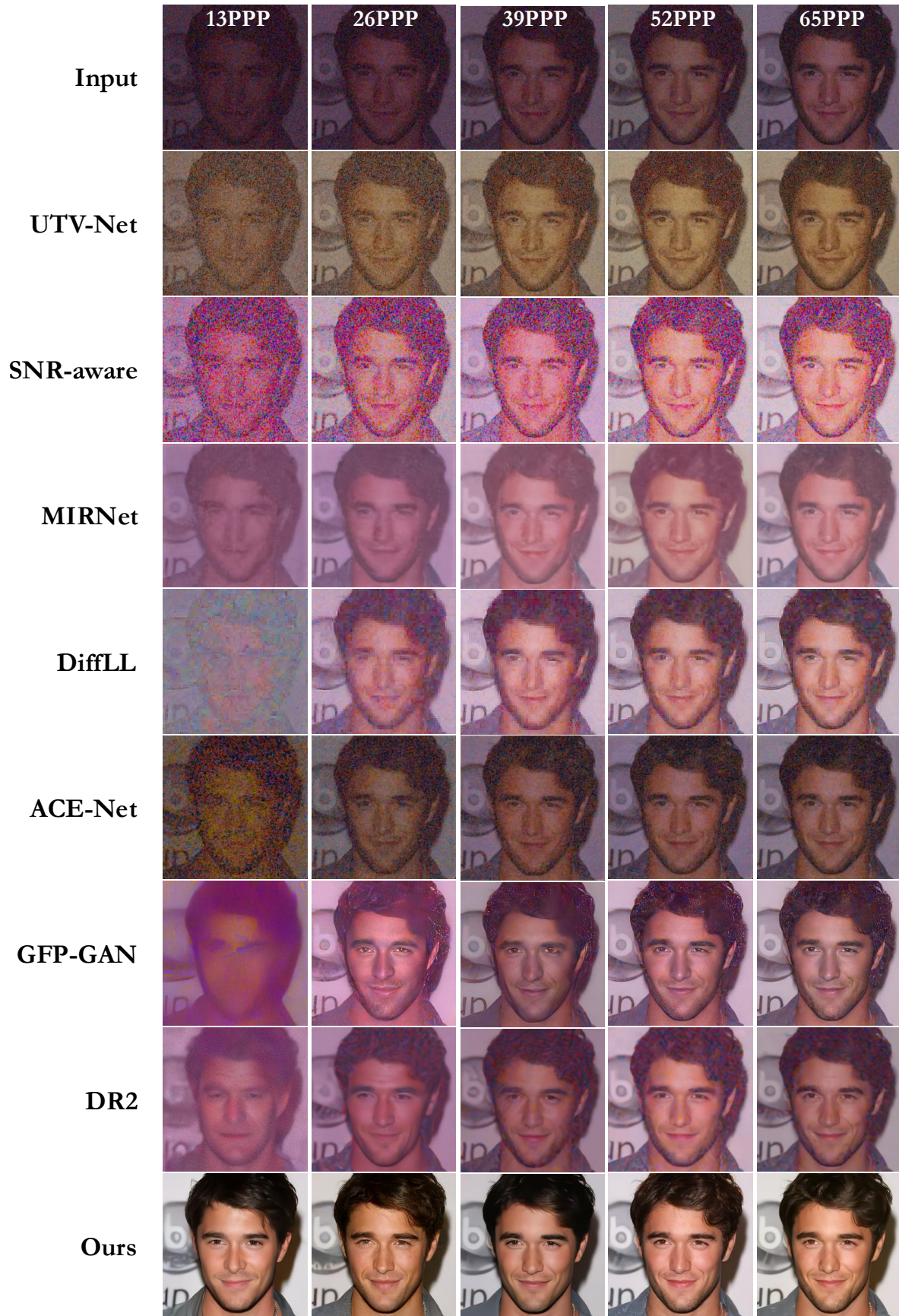


Figure 17. Visual comparison on CelebAMask-10 test set. Zoom in for the best visual experience.

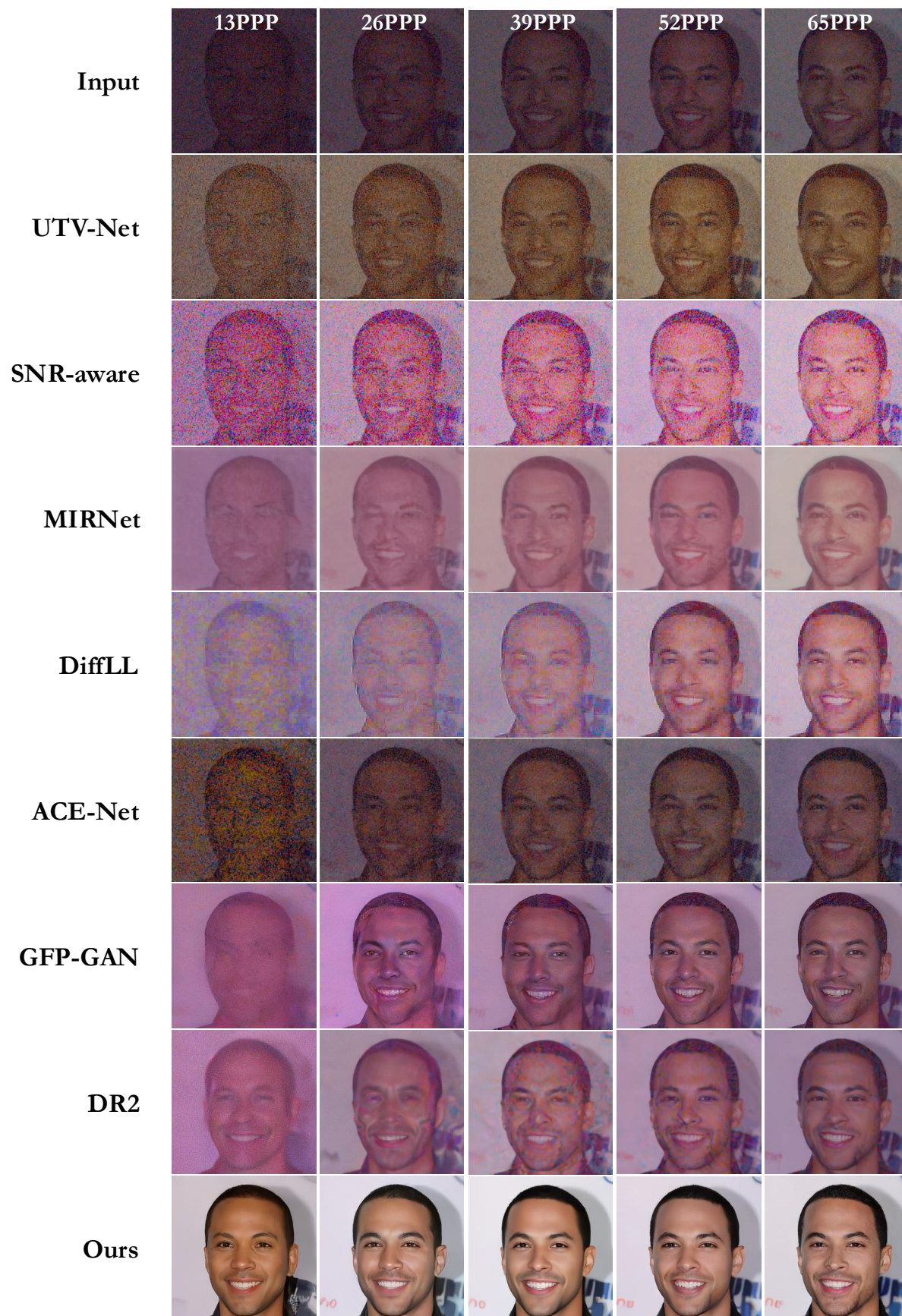


Figure 18. Visual comparison on CelebAMask- HQ test set. Zoom in for the best visual experience.

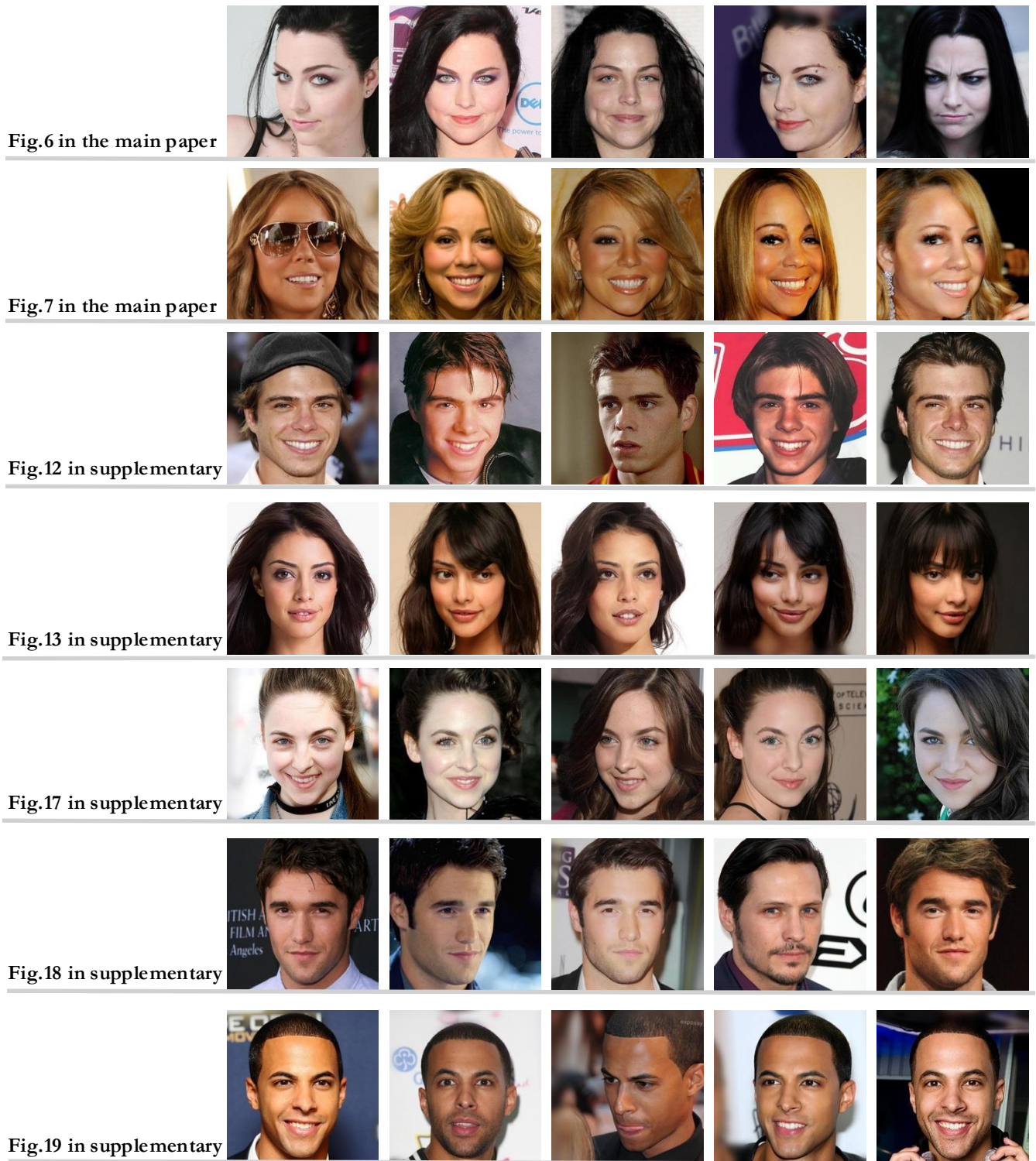


Figure 19. Gallery samples of testing persons appeared in the main paper and supplementary materials.